Heliyon 10 (2024) e30871

Contents lists available at ScienceDirect

Heliyon

journal homepage: www.cell.com/heliyon

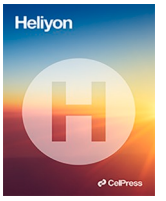

Research article

Investigation of mechanical strength and structure of corneal graft-host junction

Sai Naga Sri Harsha Chittajallu [a,b,c], Himanshu Gururani [a], Saumya Jakati [d], Sayan Basu [e], Pravin Krishna Vaddavalli [f,*], Kwong Ming Tse [b], Viswanath Chinthapenta [a,**]

[a] Department of Mechanical and Aerospace Engineering, Indian Institute of Technology Hyderabad, Hyderabad, India
[b] Department of Mechanical and Product Design Engineering, Swinburne University of Technology, Melbourne, Australia
[c] Centre for Technology Innovation, L V Prasad Eye Institute, Hyderabad, India
[d] Ophthalmic Pathology Laboratory, LV Prasad Eye Institute, Hyderabad, India
[e] Prof. Brien Holden Eye Research Centre, Hyderabad Eye Research Foundation, LV Prasad Eye Institute, Hyderabad, India
[f] The Cornea Institute, L V Prasad Eye Institute, Hyderabad, India

ARTICLE INFO

Keywords:
Wound dehiscence
Penetrating keratoplasty
Graft host junction
Cornea
Break starting strength
Suture retention strength

ABSTRACT

Dehiscence is a common complication of corneal transplant surgery involving separating the graft from the host eye. The present article aims to investigate fundamental insights into the mechanical and structural aspects of the graft-host junction (GHJ) of a graft that survived in a patient for 13 years after penetrating keratoplasty (PK). Additionally, it adopts the sutur retention strength (SRS) test procedure defined in ISO:7198-2016 and aims to provide a comprehensive test protocol to study the biomechanics of the GHJ in extracted PK buttons. A 9 mm corneal button with GHJ was extracted from a 46-year-old patient who underwent PK 13 years back. The strength of the GHJ was quantified using the SRS test. Corresponding control results were obtained from the SRS tests of a corneoscleral button with no history of any refractive procedure. Birefringence, histological, and scanning electron microscopy (SEM) imaging were used to visualize the microstructural details of the GHJ. The strength of the GHJ was observed to be ten times lower than the native cornea. Histopathological features, such as fragmented Bowman's layer, and fibrosis with a clear demarcation line between host and graft tissue, were observed at the GHJ, suggesting a weak bond across the GHJ. The low strength of the GHJ in PK indicates the high susceptibility of the GHJ towards wound dehiscence.

1. Introduction

Wound dehiscence is a persistent risk in patients with corneal transplants limiting the long-term integrity of the grafted tissue [1]. It

Abbreviations: PK, (penetrating keratoplasty); GHJ, (graft-host junction); SRS, (suture retention strength); BSS, (break starting strength); SEM, (scanning electron microscopy); IOP, (intraocular pressure); MK, (McCarey-Kaufman); CCT, (central corneal thickness); TC, (trephined cornea); UTM, (universal testing machine); HDMS, (hexamethyldisilazane); H&E, (Hematoxylin and Eosin); PAS, (Per-iodic acid Schiff's).

* Corresponding author.
** Corresponding author.
E-mail addresses: pravin@lvpei.org (P.K. Vaddavalli), viswanath@mae.iith.ac.in (V. Chinthapenta).

https://doi.org/10.1016/j.heliyon.2024.e30871
Received 20 January 2024; Accepted 7 May 2024
Available online 10 May 2024

involves the rupture of the scar tissue across the graft-host junction (GHJ), which can either be spontaneous [2,3] or trauma-triggered [1,4]. Wound dehiscence has been reported to occur in early and late postoperative scenarios [5]. While traumatic wound dehiscence occurs in young patients due to high-risk situations [6]. Additionally, previous studies have reported its dependency on age, high intraocular pressure (IOP), obesity, postoperative use of steroids, corneal edema, and wound profile [1,2,4,7].

Numerous studies have reported an abnormal collagen disposition in the GHJ post-penetrating keratoplasty. Hayes et al. [8] found a clear distinction between the graft and the host tissue after 13 years of penetrating keratoplasty (PK) using X-ray scattering and electron microscopy. Dawson et al. [9] also reported a similar finding using histopathological analysis of corneal wounds. Lang et al. [10] conducted clinicopathologic studies on the post-mortem eyes that underwent keratoplasty. They suggested that a lack of adherence between the host and the graft tissue may weaken the wound and affect corneal astigmatism. Incarceration of Bowman's layer [11] and Descemet membrane [12] were reported as the stromal defects that weakened the GHJ after keratoplasty. A recent study by Boote et al. [13] quantified the collagen disposition in the GHJ of the PK buttons. They found a significant change in the alignment (size and spatial order) of the collagen fibrils in the GHJ, suggesting inadequate wound healing, which may influence the long-term integrity of the PK graft. Notably, the abnormal fibrous architecture across GHJ limits the integrity of the PK graft, causing it to rupture. Therefore, the biomechanics of GHJ in PK is crucial in understanding wound dehiscence.

Various studies have been reported to understand the wound strength in the cornea using animal models. The effect of topical drugs on the tensile strength of the ex-vivo corneal wounds in New Zealand white rabbits has been reported previously [14,15]. Condon and Hill [16] measured the wound strength in the rabbit cornea using eye globe distention by raising intraocular pressure and excising the corneal strip with the wound. A similar study on rabbit eyes by Gasset and Dohlman [17] depicted differences in the tensile strength of the central and peripheral corneal wounds. Simonsen et al. [18] conducted tensile testing on ex-vivo human eyes extracted from cataract patients. They observed the tissue rupture across the wounded sites, suggesting lower strength of the scar tissue than the native tissue.

Considerable evidence in the literature supports the multifaceted etiology of the wound characteristics and has indicated the weak nature of corneal scars. Techniques such as histopathology, scanning electron microscopy (SEM) imaging, and X-ray diffraction have been utilized to comprehend the structural anomalies in corneal scars for both animal and human tissues. Further, the mechanical strength of the corneal wounds has been characterized using eye globe distention and conventional tensile testing of excised corneal strips containing the scars. However, as per the authors' knowledge, the biomechanics of the GHJ in PK eyes pertaining to its mechanical properties remain scarce. Intuitively, the mechanical characterization of GHJ in PK requires a special kind of tissue that contains intact GHJ post-wound healing, which is a rare event. If available, such a tissue could be utilized to quantify the strength of the GHJ and dictate the long-term integrity of a graft in a PK eye.

The current study delves into the mechanical strength and structural characteristics of the GHJ within a corneal button extracted from a patient who underwent penetrating keratoplasty 13 years ago. Typically measuring between 1 and 2 mm in thickness and situated at the corneal periphery, the GHJ poses challenges in accurately quantifying its strength through eye globe distention and conventional strip extensiometry. Notably, wound dehiscence in a penetrating keratoplasty eye reflects a typical fracture pattern where the tissue ruptures along this GHJ. Given these limitations and the occurrence of wound dehiscence, the study adopts the suture retention strength (SRS) test procedure to examine the mechanical resilience of the GHJ. Küng et al. [19,20] introduced SRS tests for ophthalmic tissues, where SRS is defined as the load corresponding to the complete tissue rupture [21]. The similarities between tissue rupture along GHJ and specimen rupture during the SRS test favor the rendition of the SRS tests' parameters as the strength of the GHJ. In the SRS tests, Pensalfini et al. [22] have introduced an additional load point known as break starting strength (BSS), where the visible rupture initiates. BSS is a vital parameter for ophthalmic tissues as any small opening in the tissue could reduce the intraocular pressure and leads to hypotony (IOP lower than 5 mm Hg). Therefore, the authors adopt a hybrid suture retention strength (SRS) test given by Küng et al. [20,23] and Pensalfini et al. [22] to evaluate the strength of the GHJ in the obtained PK button. For comparison with the native tissue, the SRS of the corneoscleral button with no history of refractive surgery is also evaluated in the current study.

The GHJ in PK demonstrates variations in the arrangement of collagen fibers. In this study, a novel approach was employed to scrutinize the structural aspects of the GHJ, aiming for a deeper comprehension of the observed mechanical behavior during the SRS tests. Examination of the PK button's structure involved employing birefringence, histopathology, and SEM analyses. Identification of the GHJ within the PK button was achieved through the utilization of the digital photoelasticity technique, which enables the comprehensive measurement of birefringence across the entire cornea [24]. Histopathology and SEM imaging provided detailed information concerning structural changes at various depths and the morphologies of the torn specimens following the SRS tests.

The following article is composed as follows: Section 1 gives an overall perspective on wound dehiscence and its association with the biomechanics of the GHJ in a PK eye. Section 2 elucidates the experimental methodology used to understand the mechanical and structural properties of the GHJ. Section 3 showcases the strength of the GHJ and its structural characteristics. Section 4 discusses the implication of GHJ strength on the long-term integrity of the PK graft and highlights the importance of biomechanical characterization of the GHJ in-vivo. Lastly, section 5 concludes the study.

2. Materials and methods

The following section elucidates the experimental methodology to investigate the mechanical properties and structural features of the GHJ. The SRS test was used to characterize the mechanical behavior of the GHJ. The structural characterization was performed using digital photoelasticity, histopathological analysis, and SEM. Finally, the SRS of the GHJ was compared with that of the control corneas (native corneal tissue).

The present study was performed under the ethical approvals obtained from the ethical committees of L V Prasad Eye Institute,

Hyderabad, India, Indian Institute of Technology (IIT), Hyderabad, India, and the Swinburne University of Technology, Melbourne, Australia. The details of the ethical approvals are provided in the declaration section.

2.1. Materials

A 46 years old male with a history of unilateral PK performed in the left eye 13 years before visited L V Prasad eye institute Hyderabad, India, with a watery eye. The slit lamp examination confirmed graft failure in the left eye. The patient's left eye was identified with stromal perforation, diffuse microcystic edema, and an elevated IOP of 29 mm Hg (See supplementary image). A 9 mm corneal button (PK button) was extracted from the patient to perform repeat keratoplasty. Fig. 1(a) shows the GHJ at the 7.5 mm diameter of the extracted button. The extracted button was immediately kept in the McCarey-Kaufman (MK) medium adhering to tissue handling guidelines of Eye Banking Standards of India 2020 [25].

Further, one disease-free human cadaver corneoscleral button (cornea ID as per eye bank: 1482OD) was obtained from the Ramayamma International Eye Bank of L V Prasad Eye Institute, Hyderabad, India, for collecting the control data. A central corneal thickness (CCT) value of less than 600 μm was chosen as an inclusion criterion [26,27] for the control cornea. The chosen CCT ensures that the tissue is not over-hydrated. Further, the data in the present study was not normalized with respect to age and sex as those details of the donor of the grafted tissue were not available.

2.2. Specimen preparation

Fig. 1(a) illustrates the sample preparation procedure for the present investigation. The PK button was dissected into two halves (H_1 and H_2). The right half (H_1) was used for histopathological analysis of the corneal cross-section, and the left half (H_2) was imaged in an in-house developed polarimeter to collect its birefringence property known as isoclinic or slow-axis orientation (see Fig. 1(a)). Later, the left half was dissected into three specimens (H_2S_1, H_2S_2, H_2S_3) of equal size for SRS tests (see Fig. 1(a)). The remnants of the SRS tests were then imaged via SEM for fractography.

The control results against the strength of the GHJ were obtained via SRS tests of the corneoscleral button. A 9.5 mm diameter central portion was mechanically punched out from the control corneas using a stainless-steel trephine (see Fig. 1(b)). The control cornea was dissected into six equal parts (see Fig. 1(c)), followed by SRS tests. The nomenclature for the six samples is given as 1482OD_TC# (TC: Trephined Cornea and # represent sample number 1, 2 …,6).

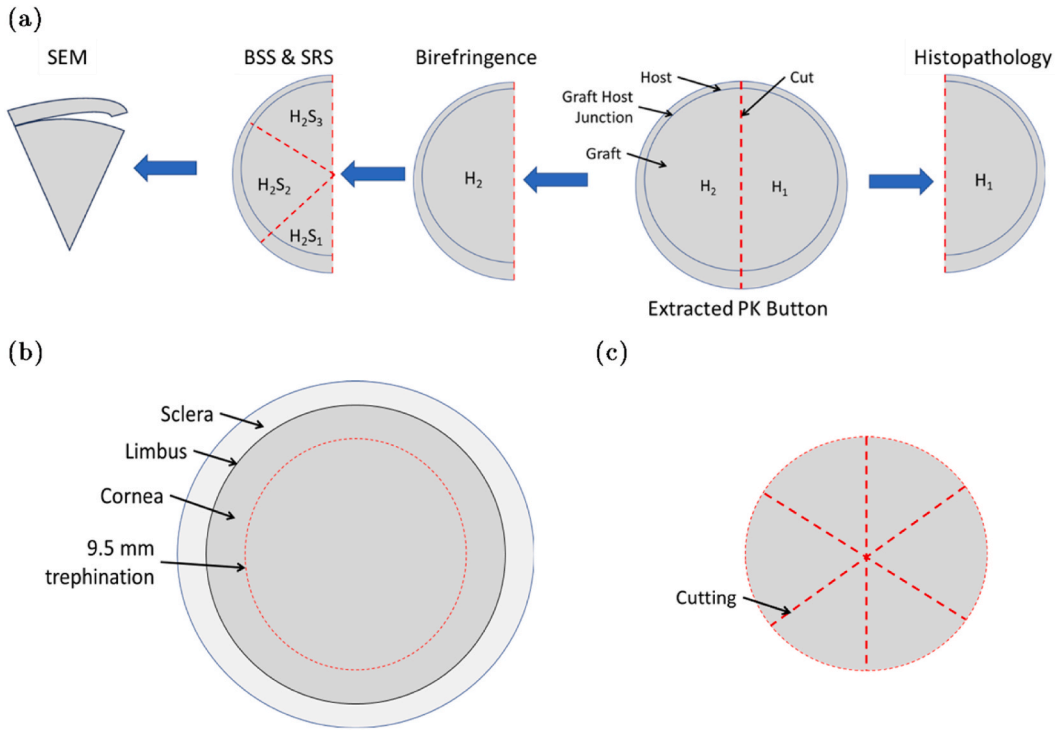

Fig. 1. (a) Pictorial representation of different geometrical segments of the extracted PK button used for different characterization techniques, (b) corneoscleral button (1482OD) for SRS control tests with trephination dimensions, and (c) Control trephine dissection into six specimens (1482OD_TC#, #: 1,2, .., 6) for SRS tests.

2.3. Digital photoelasticity

The extent of the GHJ in the specimen H_2 was assessed by measuring its birefringence using digital photoelasticity. Based on a generic circular polariscope (see Fig. 2(a)), an experimental setup (see Fig. 2(c)) was used to measure the isoclinic phase map of the specimen H_2. The isoclinic phase map gives the overall distribution of the collagen fiber in the cornea.

The specimen H_2 was mounted on an in-house designed artificial anterior chamber (see Fig. 2(b)). The anterior and the posterior side of the chamber was filled with a balanced salt solution to negate the refractive effects due to corneal curvature and induce intraocular pressure (IOP), respectively (see Fig. 2(b)). Then, the anterior chamber was placed between the first and the second quarter waveplates (see Fig. 2(c)). Four birefringence images (i_1 to i_4) of the mounted tissue were captured by a digital camera according to the polarization-stepping algorithm [28] in Table 1. These images were then post-processed using a phase unwrapping algorithm to generate a full-field isoclinic phase map (slow axis orientation) of the cornea [28]. The elaborated details on the methodology used for birefringence imaging of the cornea are given in the recent work by Gururani et al. [29].

2.4. Suture retention strength (SRS) tests

The SRS tests were performed on the universal testing machine (UTM) (Model 5944, Instron, USA) equipped with a 50 N load cell. Fig. 3(d) shows the loading of the specimen in the present study. In the present study, 6–0 vicryl sutures (M/s. Ethicon, India) were used for performing SRS tests for their ease of handling [20,23]. Before mounting the specimen, the suture was inserted 1 mm from the trephined edge of the sample (see Fig. 3(b)) for the controls (1482OD_TC#). It is important to note that the suture bite is placed at the GHJ in the specimens H_2S_1, H_2S_2 and, H_2S_3, as depicted in Fig. 3(a). Then, the specimen was mounted on the stationary arm of the

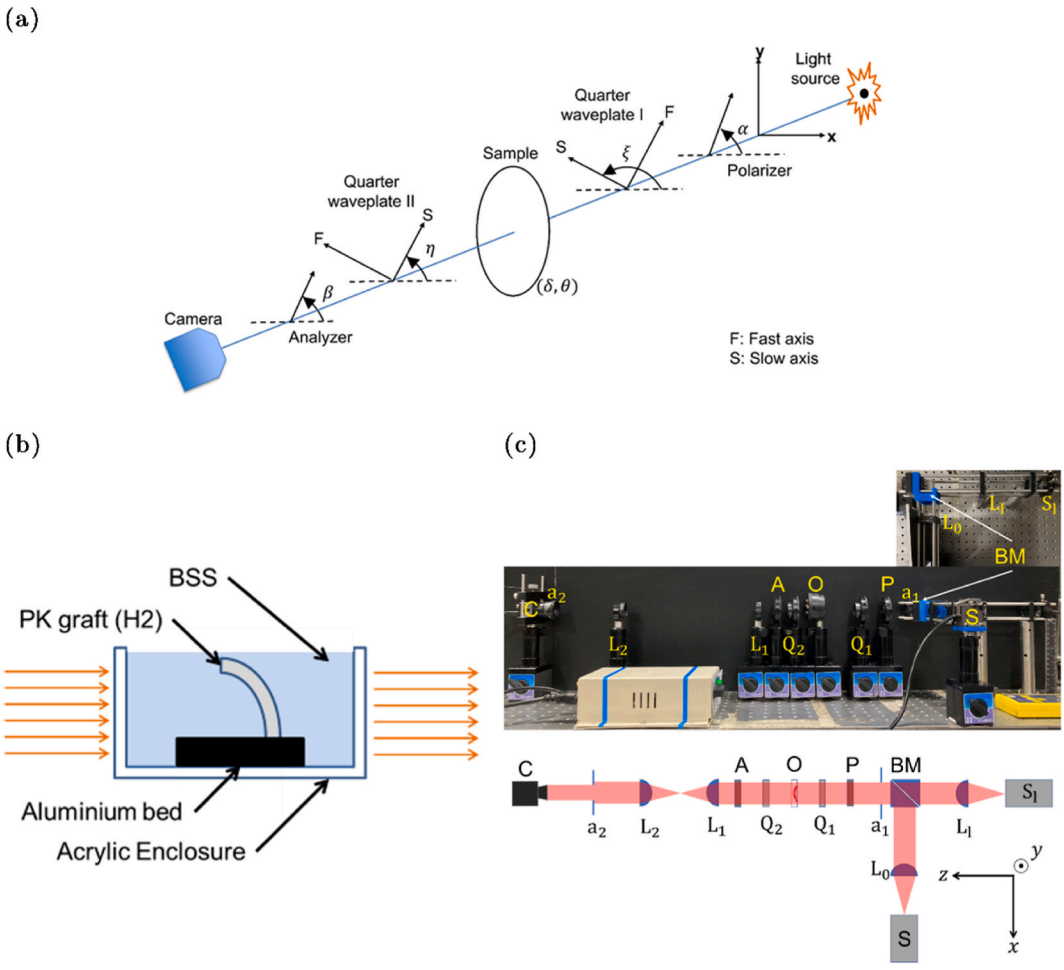

Fig. 2. (a) Generic polariscope schematic, (b) test cell schematic used for imaging control corneoscleral buttons, and (c) The experimental setup of the polariscope. The components of the setup are as follows: S: LED Source, S_l: LASER source, BM: Beam splitter, a_1: aperture, P: Polarizer, Q_1: Quarter waveplate I, O: Object, Q_2: Quarter waveplate II, A: Analyzer, L_1: Plano-convex lens I, L_2: Plano-convex lens II, a_2: aperture, C: Sensor, L_0: Plano-convex lens (LED arm), L_l: Plano-convex lens (LASER arm).

Table 1
Polarization-stepping algorithm used to evaluate birefringence properties of the cornea.

α Pol	ξ QWPI	η QWPII	β Ana	Intensity Equation
$\frac{\pi}{2}$	–	–	0	$i_1 = i_b + i_a\left[\sin^2\frac{\delta}{2}\sin^2(2\theta)\right]$
$\frac{5\pi}{8}$	–	–	$\frac{\pi}{8}$	$i_2 = i_b + i_a / 2\left[\sin^2\frac{\delta}{2}(1-\sin(4\theta))\right]$
$\frac{3\pi}{4}$	–	–	$\frac{\pi}{4}$	$i_3 = i_b + i_a\left[\sin^2\frac{\delta}{2}\cos^2(2\theta)\right]$
$\frac{7\pi}{8}$	–	–	$\frac{3\pi}{8}$	$i_4 = i_b + \frac{i_a}{2}\left[\sin^2\frac{\delta}{2}(1+\sin(4\theta))\right]$

UTM using 800-grit sandpaper to avoid slippage during the tests. A customized mount visualized in Fig. 3(e) was designed to hold the sutures on the UTM arm to facilitate suture pull-out. After fixing the sutures on the customized mount, the sutures were pulled at 3 mm/min [19,20,30]. The complete schematic of the experimental setup for SRS tests is given in Fig. 3(f). A video of the specimen deformation was also recorded at 10× magnification at a frame rate of 30 fps as depicted in Fig. 3(g).

According to ISO:7198, the BSS and SRS are two parameters that dictate the breaking pattern of the tissues. The BSS defines the load at which the initial tear is visible (depicted as black squares in load vs. extension curves; see SRS results). Likewise, the load corresponding to the complete tear of the sample is known as SRS (depicted as red dots in load vs. extension curves, see SRS results). Both BSS and SRS were noted for PK as well as control. The BSS was identified from the captured video at the time frame corresponding to the first tear in the sample.

2.5. Fractography sample preparation

The remnants from SRS tests (see Fig. 3(c)) were fixed in a freshly prepared 2.5 % glutaraldehyde (in 0.1 M phosphate buffer solution) solution for microstructural analysis for 24 h. Later, for secondary fixation (before imaging), the samples were post-fixed in 1 % osmium tetra-oxide (M/s. Sigma Aldrich, St. Louis, USA) for 2 h. The samples were washed with phosphate buffer (PB) buffer thrice and then subjected to gradual dehydration (20 %, 35 %, 50 %, 75 %, 95 %, 100 %) followed by dehydration with hexamethyldisilazane (HMDS) (Sigma Aldrich, St. Louis, USA) twice for 10 min each. The HMDS was decanted, and the treated samples were allowed to air dry. The samples were gold-sputtered and observed for microstructural analysis using JSM-7610F ultra high-resolution Schottky Field Emission Scanning Electron Microscope.

2.6. Histopathology sample preparation

The sample was fixed overnight in 10 % neutral buffered formalin and processed in the automated tissue processor (Leica TP 1020) as per standard laboratory protocol. The sample was embedded, sectioned at four-micron thickness, and stained with Hematoxylin and Eosin stains (H&E) and Per-iodic acid Schiff's stain (PAS).

3. Results

The following section elucidates the structural various in the GHJ via birefringence mapping of the specimen H_2, followed by the results of the suture retention strength tests for PK specimens (H_2S_1, H_2S_2, and H_2S_3) and control specimens (1482OD_TC#). The structural features of the GHJ are also shown via histopathological images of the right half (H_1) of the PK button. The SEM images of the torn surfaces of the PK specimens after SRS tests are also presented.

3.1. PK button birefringence

Fig. 4(a) shows the polarization-stepped (i_1 to i_4) birefringence images of the PK specimen H_2. The images i_1 to i_4 exhibit variation in the intensity across the entire domain. However, a qualitative inspection of the images i_1 to i_4 reveals an abrupt jump in the intensity in the periphery of the specimen (annotated by a yellow in Fig. 4 (a)), which is typically not seen in the native cornea. Naturally, the existence of the GHJ at the periphery impacts the polarization characteristics of incoming light, resulting in a noticeable shift in intensity. It's crucial to recognize that the GHJ lacks symmetry concerning the specimen boundary, evident in the greater presence of host tissue at location L_1 compared to L_2.

Fig. 4(b) shows the unwrapped isoclinic phase map obtained by processing the images, i_1 to i_4 (see section 2.3). The isoclinic map of the specimen exhibits typical features, such as the presence of π-jump and isotropic points, similar to the native eye [24]. A distortion in the isoclinics can be observed at the location L_1, indicating the presence of GHJ (annotated by a black dotted curve in Fig. 4(b)). However, the isoclinic phase at L_2 does not clearly indicate the presence of GHJ. It is clear that an asymmetric trephination of the PK button has resulted in the uneven disposition of the GHJ depicted by the birefringence images of H_2.

After birefringence imaging, the specimen H_2 was dissected to prepare three samples for SRS tests. Due to the uneven trephining, the location L_1 (maximum amount of host tissue) was present in H_2, and location L_2 (minimum amount of host tissue or no host tissue)

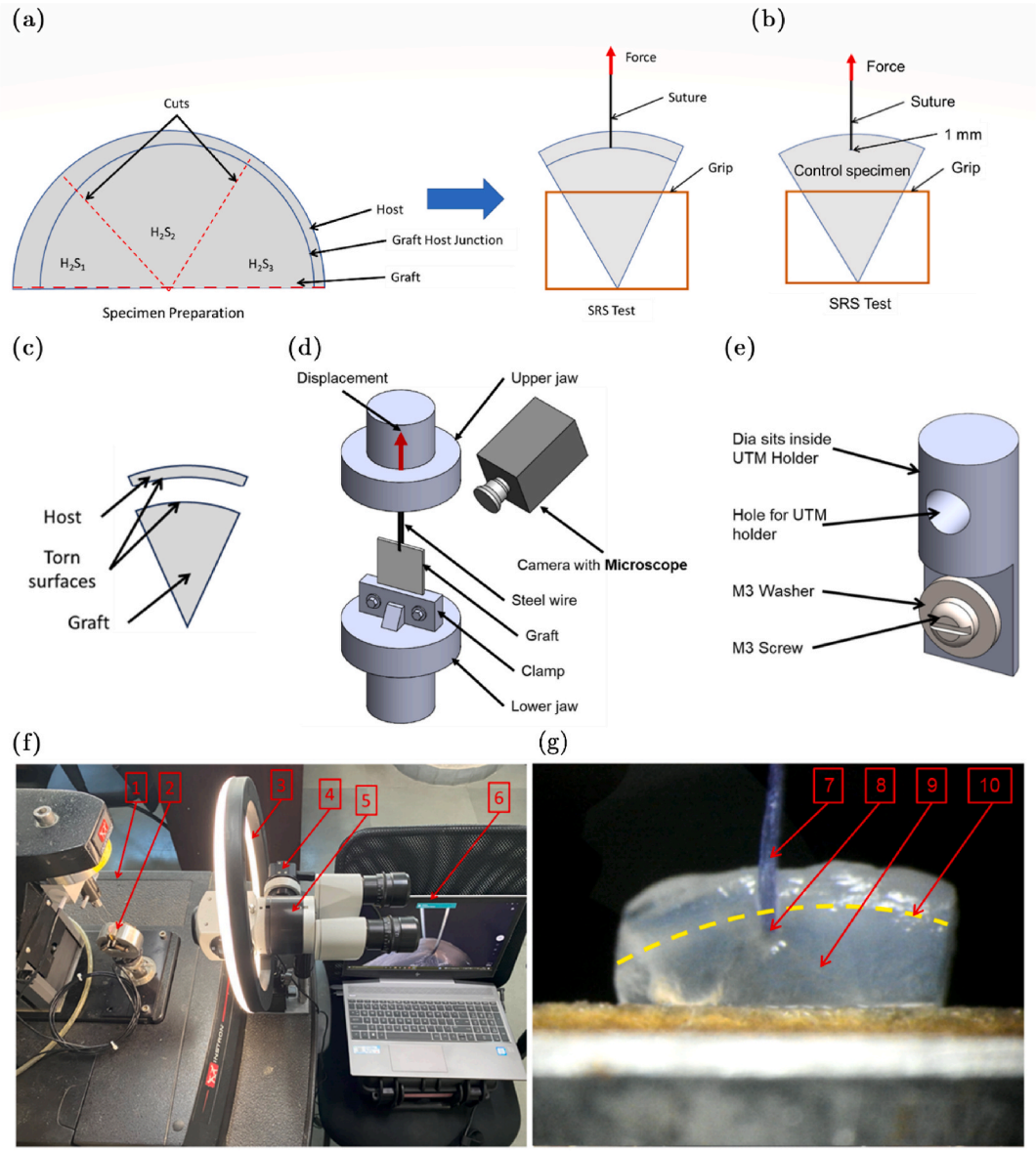

Fig. 3. (a) SRS specimen preparation from PK button and its loading condition in SRS test, (b) loading condition for the SRS control specimens, (c) Tron specimen post SRS test, (d) SRS experiment schematic, (e) customized suture holder for SRS test, (f) Experimental setup for evaluating BSS it contains 1 UTM, 2 specimen, 3 external illumination, 4 camera attached to 5 a microscope and experiment is captured in a laptop 6, and (g) Specimen visualized on the screen containing 7 6-0 vicryl suture, 8 tear initiation location due to pulling and 9 is extracted PK button, and 10 GHJ is marked with a discontinuous yellow line. (For interpretation of the references to colour in this figure legend, the reader is referred to the Web version of this article.)

was present in H_2S_3.

3.2. *Suture retention strength: PK button vs. control corneal button*

In the present study, the SRS test was used to measure the strength of the GHJ. Fig. 5(a) gives the load versus extension behavior of the GHJ for the specimens H_2S_1, H_2S_2, and H_2S_3. The specimens H_2S_1, H_2S_2, and H_2S_3 exhibit the typical J-shaped curve up to a load of approximately 0.15 N (see Fig. 5(a)). During suture pull-out, the first kink in the load-extension curve (annotated by black squares, see Fig. 5(a)) is marked, and the corresponding load value (BSS/tear initiation) is noted. The BSS of H_2S_1 and H_2S_2 is observed to be 0.1 N, and H_2S_3 is 0.2 N. The snapshot of the specimen at the instant of the first kink was also captured (see left side of Fig. 5(a)).

The load increases till the SRS point for H_1S_1 and H_2S_2, depicting the resistance of the GHJ against tear. The SRS of H_2S_1 and H_2S_2 is approximately 0.4 N. Once the SRS is reached, the tear in the specimen starts to propagate along the weak interface (GHJ). The plateau

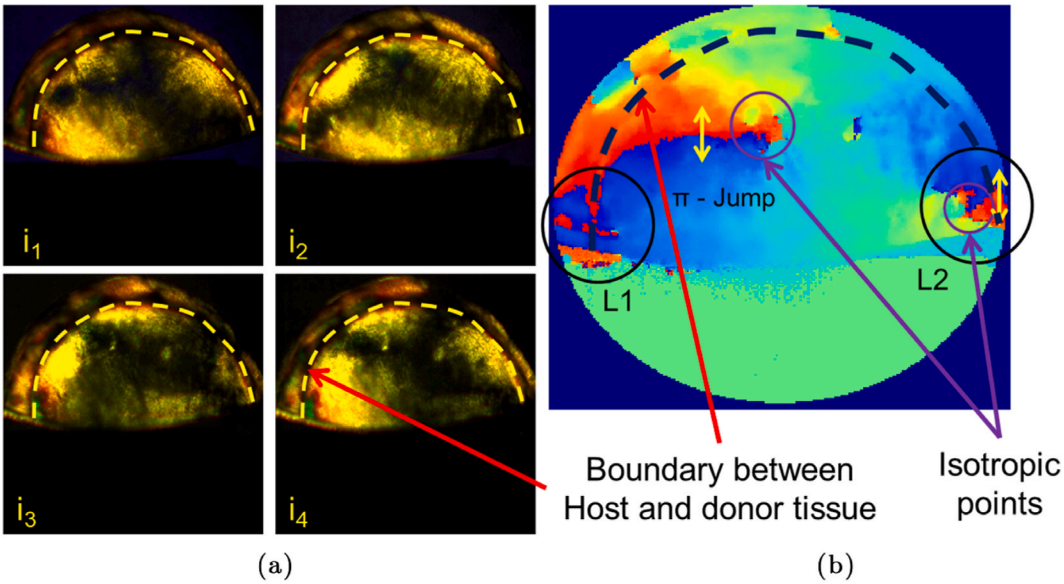

Fig. 4. (a) Four-step images of the left half H_2 of the extracted PK button where GHJ is marked with a discontinuous yellow line and (b) the corresponding isoclinic map of H_2 evaluated by phase unwrapping algorithm. It is important to note that the GHJ is marked with a discontinuous black line in the isoclinic phase map. L_1 and L_2 are the locations of GHJ identified with distorted phase data. (For interpretation of the references to colour in this figure legend, the reader is referred to the Web version of this article.)

region of the load-extension curve depicts the tear along the GHJ. The SRS values annotated by red dots and corresponding specimen snapshots were also captured for all the specimens (see right side of Fig. 5(a)).

Contrarily, after BSS, the specimen H_2S_3 attains an SRS of 1 N due to the contribution of the graft tissue in sustaining the load during suture pull-out. Then, the load-extension behavior of H_2S_3 exhibits a sudden load drop followed by the plateau region depicting a tear along the interface (see right side of Fig. 5(a)).

Fig. 5 (b) gives the load vs. extension profiles for the six-sectioned control corneas. The images corresponding to the BSS and SRS for the samples 1482OD_TC# are shown on the left and right sides of Fig. 5 (b), respectively. Due to the slippage of one of the six specimens during the test, only five curves are given in Fig. 5(b).

Similar to the PK specimens, the load vs. extension curves of the control specimens depicts a typical J-shaped curve up to 2 N (see Fig. 5 (b)), commonly observed in soft tissues. This is missing in one of the specimens (see Fig. 5(b), specimen 1482OD_TC1), probably due to the specimen mounting issues. The BSS and SRS of the control specimens were calculated similarly to the PK specimens. The control cornea exhibits a BSS and SRS of 1.289 ± 0.185 N and 4.403 ± 0.287 N, respectively. Unlike the PK specimens, the plateau regions are not present in the load vs. extension curves of the control specimens (see Fig. 5(b)), possibly due to the absence of the GHJ.

3.3. Fractography of the SRS specimen

In the present section, the torn surfaces of the SRS test remnants (H_2S_1, H_2S_2, and H_2S_3) were analyzed using an SEM to understand the morphological characteristics of the tearing. Fig. 6(a) shows the SEM micrographs of the torn surfaces of the host (towards left) and graft (towards right) sections of the specimens at 1000x and 5000x. At a magnification of 1000x, the specimens H_2S_1 and H_2S_2 exhibited a regular lamellar tear morphology with collagen lamellae sheets placed over each other. On the contrary, H_2S_3 depicted a distorted morphology for both host and graft surfaces. A detailed view of the torn surfaces for H_2S_1 and H_2S_2 is shown at 5000× magnification in Fig. 6(a). The dense fiber bundles organized in a wavy pattern are annotated with triangles (see Fig. 6(a)) were in the host and graft surfaces of the specimen H_2S_1 and H_2S_2. An elaborated view of these fiber bundles is shown at 10000X (see Fig. 6(b)).

Contrarily, the specimen H_2S_3 exhibited a fiber-pull-out morphology, as indicated by the arrows in Fig. 6(a) for both the host and graft surfaces. The fiber pull-out in H_2S_3 can be appreciated from the magnified view of the graft surface of the specimen H_2S_3 at 10000X (see Fig. 6(c)).

3.4. Histopathology of the PK button

Fig. 7 shows the histopathology images of the PK specimen H_1. The rightmost location L_1 in Fig. 7(a) depicts a transition in the fibrous disposition of the stroma. The presence of Bowman's layer fragmentation, Descemet's membrane split, and fibrosis along the surgical scar can be observed in the magnified view of L_1 (see Fig. 7(c)).

Unlike L_1, the leftmost location L_1 doesn't indicate the presence of any fibrous transition in the stroma (see Fig. 7(a)). However, the magnified view of L_2 revealed the fragmentation of Bowman's layer (see Fig. 7(b)).

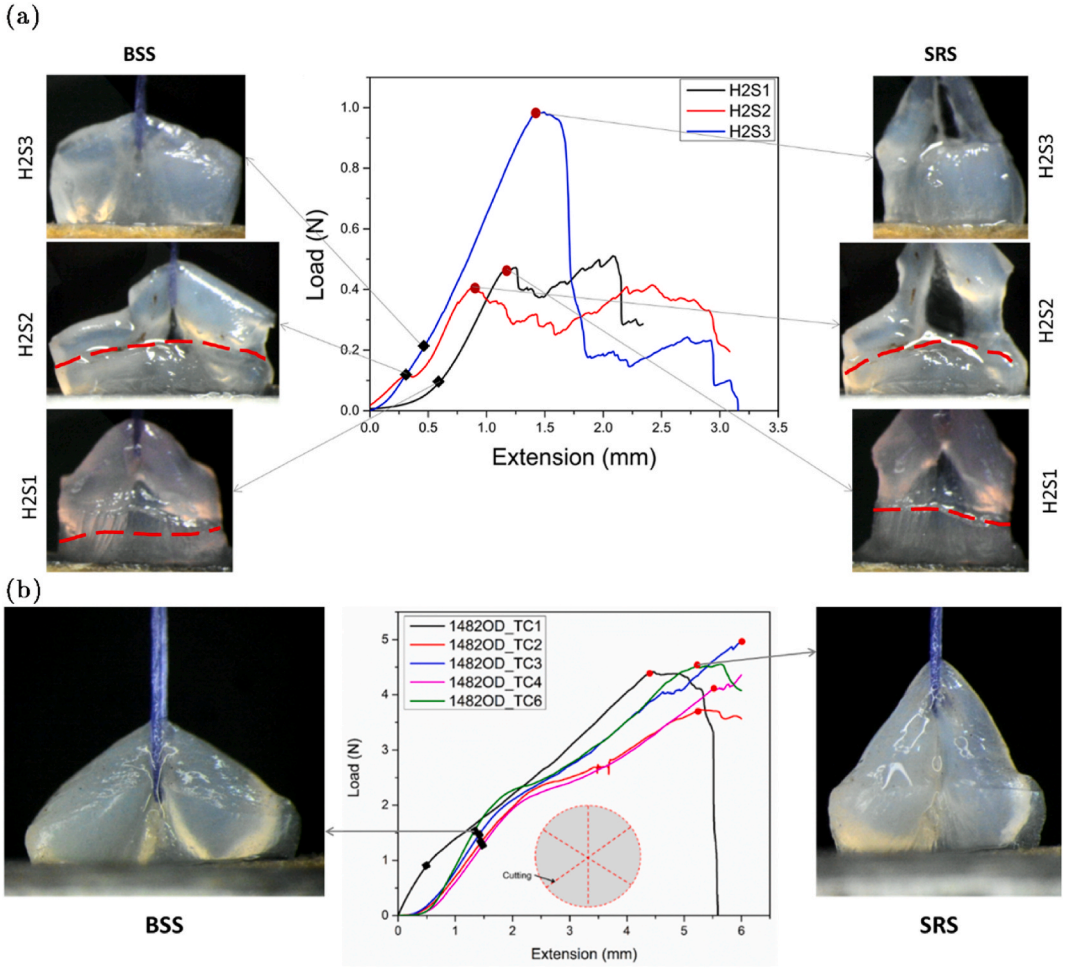

Fig. 5. Mechanical behavior of the PK and control specimens. (a) Load vs. extension curves of the specimens H_2S_1, H_2S_2 and H_2S_3 and (b) Load vs. extension curves of the control specimens. The black squares and red dots marked on the load–extension curves represent BSS and SRS, respectively. The specimen snapshots while mechanical testing corresponding to BSS and SRS are shown on the left and right sides, respectively, for both PK and control specimens. (For interpretation of the references to colour in this figure legend, the reader is referred to the Web version of this article.)

4. Discussion

Despite being a highly effective long-term treatment option for patients with advanced keratoconus, dystrophies, etc., PK patients are always at risk of graft failure due to wound dehiscence. Wound strength is an important property that dictates the long-term stability of the graft. A large amount of evidence based on structural analysis in the literature suggests that the GHJ never regains its full strength [11–13,18]. However, the quantification of the GHJ's mechanical strength remains to be established. The present study is the first of its kind to investigate the mechanical strength of the GHJ of a PK graft that survived in a patient for 13 years.

In this first-of-its kind study, the mechanical strength of the GHJ in a PK graft was investigated using SRS tests and compared with the control cornea with no refractive surgery history. Digital photoelasticity was used to study the birefringence of the PK button, and SEM analysis was carried out on the remnants of the SRS tests to analyze the morphology of the torn surfaces. Likewise, histopathology analysis was carried out to understand the characteristics of the GHJ across the PK button. The birefringence of the PK button extracted using digital photoelasticity has rendered good visibility of GHJ and its variation in the button. However, this study's interpretation relies on qualitative birefringence analysis, it could be planned for future research to incorporate quantitative measurements for a more profound understanding of wound remodeling and its correlation with graft-host junction strength.

The GHJ has shown a low BSS of 0.1 N in specimens H_2S_1 and H_2S_2 and 0.4 N in the specimen H_2S_3. The higher BSS in the specimen H_2S_3 is possibly due to the higher influence of graft tissue than GHJ. It could be due to an offset in trephination while extracting the PK button, which introduced a non-uniformity in the disposition of the GHJ across the extracted button. The birefringence and histopathology images of the specimen H_2 also showed the variability in the fraction of GHJ across the PK button (see Figs. 4 and 7). The GHJ is located away from the periphery at L_1 and towards the periphery at L_2 (see Fig. 4 (a)).

It is interesting to note that the GHJ at L_1 and L_2 shows distorted isoclinic data (see Fig. 4(a)), representing an alteration in the

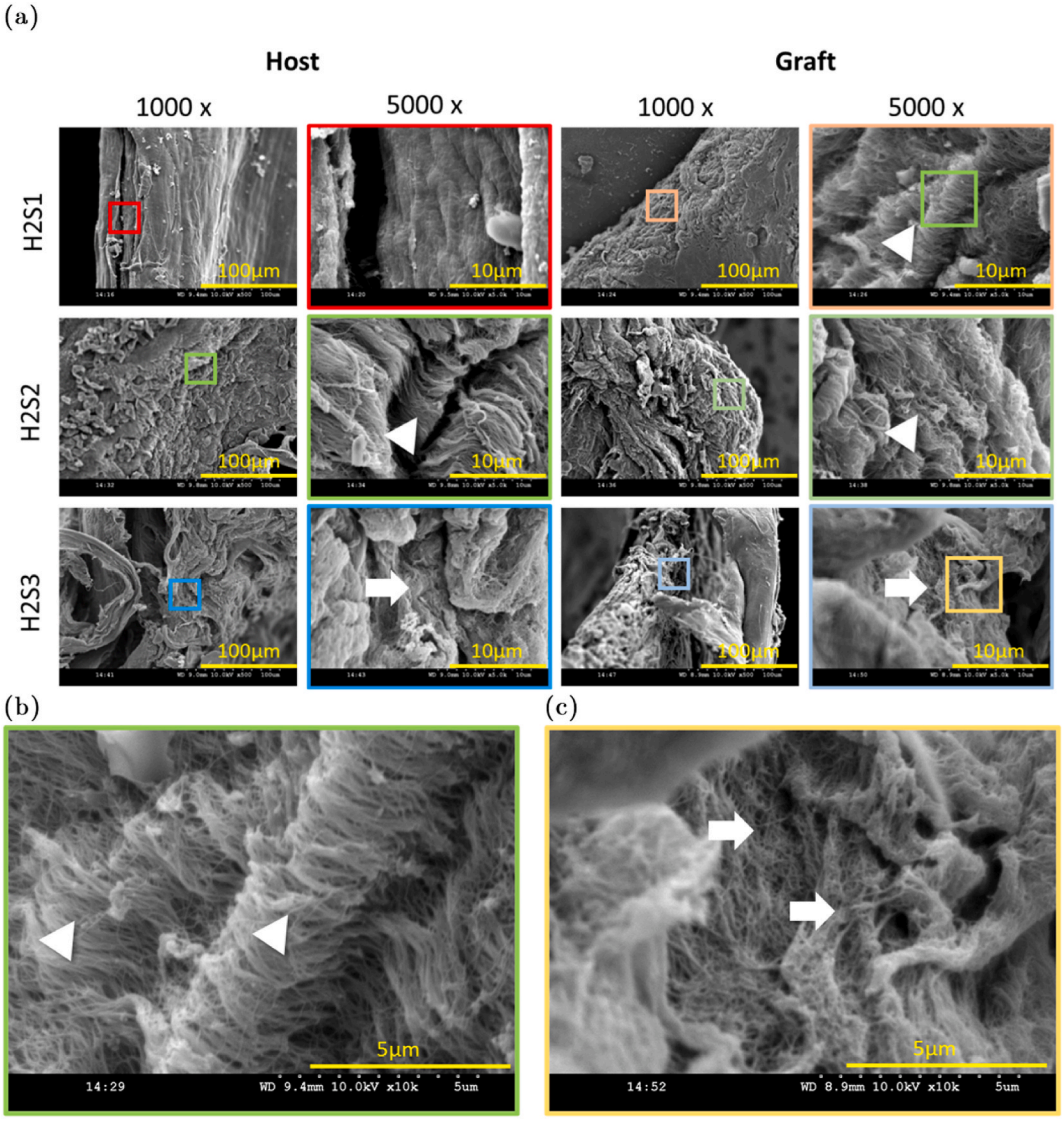

Fig. 6. SEM results of the torn specimen surfaces post SRS tests where (a) is the matrix of results of extracted PK button for both host and graft at a magnification of 1000x and 5000x, (b) wavy collagen fiber morphology on GHJ in specimens 1 and 2, and (c) pulled out fiber morphology from specimen 3. Here wavy fibers are marked with triangular pointers and pulled-out fibers are marked with arrowhead pointers.

collagen fiber arrangement. This altered fibrillar disposition can be appreciated from the presence of wound healing features like Bowman's layer fragmentation, Descemet's membrane split, and scar with fibrosis (demarcation line between the graft and host tissue) at L_1 and Bowman's layer fragmentation at L_2 (see Fig. 7(a)). It is important to note that dissimilarity in the disposition of GHJ in the specimen H_2 might have influence the SRS of the specimens H_2S_1, H_2S_2, and H_2S_3. The higher value of SRS for specimen H_2S_3 indicates a greater influence of host tissue than the GHJ.

The load–extension curves of specimens H_2S_1, H_2S_2, and H_2S_3 showed a typical tear characteristic in the form of a plateau region after reaching the SRS point. The plateau represents crack propagation along the interface (GHJ, region of lowest strength). Unlike specimen H_2S_1, H_2S_2, specimen H_2S_3 exhibited an instant load drop followed by the plateau. The load rise in H_2S_3 up to an SRS of 1 N can be attributed to the influence of graft tissue in suture retention. Then, load drop can be attributed to the instantaneous participation of the GHJ in resisting the tear during the suture pull-out, followed by a tear along the weak interface (GHJ).

The difference in the load-extension profiles of the PK specimens can also be appreciated by the morphological features of the torn surfaces of H_2S_1, H_2S_2, and H_2S_3 (see Fig. 6(a)). Specimens H_2S_1 and H_2S_2 exhibited a wavy morphology of the collagen fibers (see Fig. 6(b)) typically observed in trephined corneas [31,32], indicating due to a smooth tear along the fibrotic scar tissue. While specimen H_2S_3 depicted a collagen fiber-pull-out morphology typically observed in open-mode tearing (see Fig. 6(c)) of the skin [33, 34], fibrous scaffolds [35] and human cornea [32]. This kind of morphology can be attributed to the fragmented Bowman's layer observed at L_2 of the GHJ (see Fig. 7(a)) and absence of scar/fibrosis (clear demarcation line between host and the graft). The higher

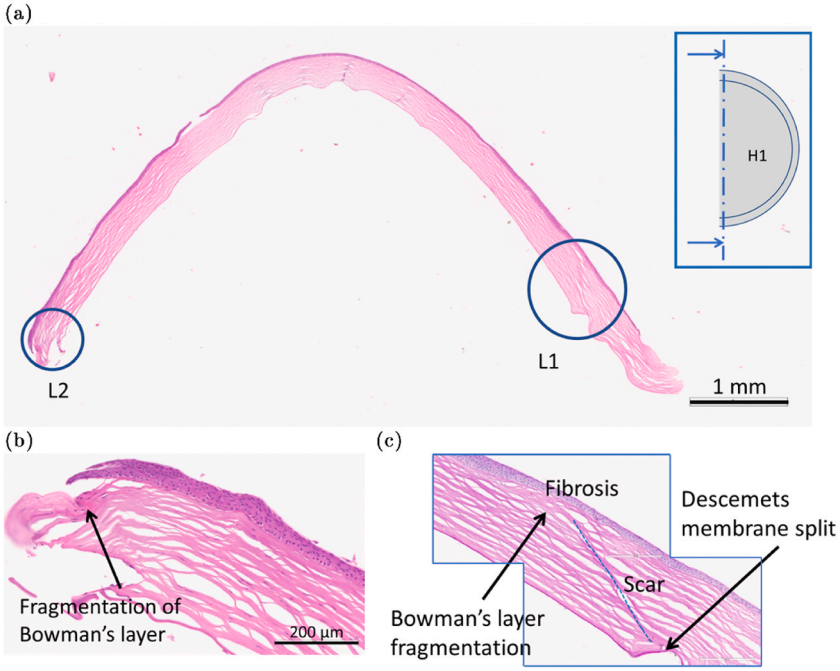

Fig. 7. Histopathology results of the PK button where (a) is the complete specimen with H&E stain and the cross-section and image plane of the H2 specimen are in the small window, (b) L2 with H&E stain, and (c) L1 with PASS stain (stitched with two images).

value of SRS for H_2S_3 and presence of Bowman's split along with the results presented in this study suggest that the tear in specimen H_2S_3 occurred in the graft part of the extracted PK button. However, the BSS of H_2S_3 is not as high as the controls due to the influence of GHJ that eventually participated in the tearing.

BSS and SRS in the control specimens were found to be ten times higher compared to the PK specimens (see Fig. 5(b) and (c)), suggesting the GHJ to be weaker than the native human cornea. This can be attributed to the microstructural remodeling at the GHJ during wound healing. When the host and graft are apposed during suturing, the open collagen fibers on the host and graft surfaces get entangled, move into the available gaps, and bend perpendicular to the suture. A recent study on collagen ultrastructure of GHJ indicated only 10 % of the remodeled collagen along the meridional direction [13], rendering the GHJ susceptible enough to dehisce. Hence, it is appropriate to mention that wound dehiscence due to trauma has been seen even after 19 years of PK [36]. No significant variation of the BSS and SRS were observed in the control specimen. Hence the control tests were limited to single specimen. Use of more corneal buttons would lead to variation in the results due to multiple factor such as age, sex, thickness, and microstructure of cornea. This makes investigation of the BSS and SRS of human cornea is extensive study and it is out of scope of the present study.

Although the patient's eye reported in the present study suffered graft rejection due to clinical features such as watery eye, perforations, and edema, the GHJ did not exhibit signs of dehiscence. However, the findings herein suggest the susceptibility of an already weakened interface (GHJ) to dehisce. Therefore, an apparent "clinically healed wound" may not sufficiently be strong to resist spontaneous loadings in in-vivo scenarios. The present study involves only one rare-to-find graft that allowed the authors to quantify the mechanical properties of the GHJ. However, the high tendency of the GHJ to open up under traumatic loadings demands in-vivo techniques that can estimate the GHJ's strength via monitoring the collagen remodeling during wound healing. The methods such as polarimetry [24,37], optical coherence elastography (OCE) [38–40], and Brillouin microscopy [41–43] can map the mechanical properties of the cornea. Utilizing these techniques for in-vivo studies is currently out of the scope of the present investigation. Incorporating these techniques in the current clinical paradigm can help assess wound remodeling after PK to identify patients at risk of wound dehiscence and manage wound stability through repair and regeneration techniques for wound healing.

In essence, this article represents the inaugural quantitative exploration of both the mechanical resilience and microstructure of the GHJ. The study's discoveries suggest that despite years of the graft remaining stable within the host eye, the GHJ isn't achieving its complete strength [44,45]. While the GHJ's strength was adequate to maintain the graft's integrity within the patient's eye, it remains vulnerable to separation or dehiscence when subjected to trauma or increased intraocular pressure due to the distinctive characteristics of the remodeled collagen observed at the GHJ [6,46].

The present study is limited to one PK button; however, it gives a good understanding of the biomechanics of the GHJ. Where birefringence of the cornea is studied using a plane polariscope to ensure the presence of the GHJ in the extracted corneal button, the SRS test was used to study the mechanical strength, and the remnants of the SRS test were analyzed using SEM to study the type of failure. Finally, histopathology analysis was used to study the presence of the GHJ. Availability of these corneal buttons is rare for studying which is a reason for limiting the current study to a single specimen. Although this study is limited to a single specimen, the quantified data supports the conclusions that the low strength of the GHJ arises from the microstructural characteristics of the

remodeled wound at the GHJ. The limitation of a single sample also arises due to the availability of the PK buttons that consist of GHJ. The sample used in the present study was extracted from a patient receiving another transplant after 13 years of graft survival. It is intuitive that availability of such kind of tissue in larger quantities is challenging. This rarity contributes significantly to the scientific value of our investigation, as it represents a singular opportunity to gain insights into characteristics of graft-host junction in the cornea.

5. Conclusion

The current study's findings offer intriguing insights into the biomechanical aspects of the GHJ following wound healing, employing a comprehensive approach encompassing mechanical analyses, histopathology, electron microscopy, and birefringence characterizations. Data from histopathology, SEM, and birefringence correspond to the observed behavior during the SRS tests, demonstrating failure characteristics across the GHJ in the PK button. SEM imaging highlighting tear characteristics during suture pull-out underscores a critical aspect of graft failure. The arrangement of remodeled collagen throughout the GHJ delineates the GHJ's predisposition to dehiscence. Moreover, this study presents an extensive test protocol for investigating the GHJ's biomechanics in extracted PK buttons, utilizing the SRS test procedure outlined in ISO:7198-2016 to quantify the GHJ's strength.

Ethics declaration

Helsinki Protocols are followed while handling, storage, and disposal of the corneal tissues used for the testing. The consent is sought from the kith/kin of the donor for medical research purposes. The current studies are performed with the ethical approval from the institutional review board from L V Prasad Eye Institute, Hyderabad (Ethics. Ref. No. 05-19-261, Dt. May 14, 2019), Institutional Ethics committee from IIT Hyderabad, Hyderabad (IEC Protocol No. IITH/IEC/2019/05/15, Dt. May 2, 2019), and Swinburne University of Technology Human Research Ethics Committee, Melbourne (Ref no. 20202695-3861, Dt. March 04, 2020).

Data availability

All data generated or analyzed during this study are included in this published article and its supplementary information files.

CRediT authorship contribution statement

Sai Naga Sri Harsha Chittajallu: Data curation, Formal analysis, Investigation, Methodology, Validation, Visualization, Writing – original draft. **Himanshu Gururani:** Formal analysis, Investigation, Methodology, Validation, Visualization, Writing – original draft. **Saumya Jakati:** Formal analysis, Investigation, Visualization, Writing – original draft. **Sayan Basu:** Conceptualization, Methodology, Supervision, Validation, Writing – review & editing. **Pravin Krishna Vaddavalli:** Conceptualization, Funding acquisition, Methodology, Resources, Supervision, Validation, Writing – review & editing. **Kwong Ming Tse:** Conceptualization, Formal analysis, Methodology. **Viswanath Chinthapenta:** Project administration, Resources, Supervision, Writing – review & editing.

Declaration of competing interest

The authors declare that they have no known competing financial interests or personal relationships that could have appeared to influence the work reported in this paper.

Acknowledgments

The authors thank Ramayamma Eye Bank of L V Prasad Eye Institute, Hyderabad, for providing the cadaver corneas for the experiments. The authors would like to express our heartfelt gratitude to Dr. Subha Narayan Rath from the Department of Biomedical Engineering, IITH, for generously providing access to his esteemed Regenerative Medicine and Stem Cell Lab. Author VC is grateful to L V Prasad Eye Institute, Hyderabad, for partial funding towards research assistantship to authors HG and SNH. The author VC acknowledges DST, SERB, the government of India, and CII for partial funding under the prime minister doctoral research fellowship scheme to author HG.

Appendix A. Supplementary data

Supplementary data to this article can be found online at https://doi.org/10.1016/j.heliyon.2024.e30871.

References

[1] F.C. Lam, M.Q. Rahman, K. Ramaesh, Traumatic wound dehiscence after penetrating keratoplasty—a cause for concern, Eye 21 (2007) 1146–1150, https://doi.org/10.1038/sj.eye.6702407.

[2] E.S. Abou-Jaoude, M. Brooks, D.G. Katz, W.S. Van Meter, Spontaneous wound dehiscence after removal of single continuous penetrating keratoplasty suture, Ophthalmology 109 (2002) 1291–1296, https://doi.org/10.1016/S0161-6420(02)01078-3.
[3] P.K. Nagra, K.M. Hammersmith, C.J. Rapuano, P.R. Laibson, E.J. Cohen, Wound dehiscence after penetrating keratoplasty, Cornea 25 (2006) 132–135, https://doi.org/10.1097/01.ico.0000179926.74780.b2.
[4] M. Palamar, Traumatic wound dehiscence after penetrating keratoplasty, Turkish J. Trauma Emerg, Surg. 22 (2016) 437–440, https://doi.org/10.5505/tjtes.2016.26963.
[5] X. Wang, T. Liu, S. Zhang, X. Qi, S. Li, W. Shi, H. Gao, Outcomes of wound dehiscence after penetrating keratoplasty and lamellar keratoplasty, J. Ophthalmol. 2018 (2018) 1–5, https://doi.org/10.1155/2018/1435389.
[6] M.A. Williams, S.D. Gawley, A.J. Jackson, D.G. Frazer, Traumatic graft dehiscence after penetrating keratoplasty, Ophthalmology 115 (2008) 276–278.e1, https://doi.org/10.1016/j.ophtha.2007.04.006.
[7] D.G. Heidemann, Oversized donor grafts in penetrating keratoplasty, Arch. Ophthalmol. 103 (1985) 1807, https://doi.org/10.1001/archopht.1985.01050120041016.
[8] S. Hayes, R. Young, C. Boote, N. Hawksworth, Y. Huang, K.M. Meek, A structural investigation of corneal graft failure in suspected recurrent keratoconus, Eye 24 (2010) 728–734, https://doi.org/10.1038/eye.2009.159.
[9] D.G. Dawson, H.F. Edelhauser, H.E. Grossniklaus, Long-term histopathologic findings in human corneal wounds after refractive surgical procedures, Am. J. Ophthalmol. 139 (2005) 168–178, https://doi.org/10.1016/j.ajo.2004.08.078.
[10] G.K. Lang, W.R. Green, A.E. Maumenee, Clinicopathologic studies of keratoplasty eyes obtained post mortem, Am. J. Ophthalmol. 101 (1986) 28–40, https://doi.org/10.1016/0002-9394(86)90461-7.
[11] J.C. Morrison, K.C. Swan, Bowman's layer in penetrating keratoplasties of the human eye, Arch. Ophthalmol. 100 (1982) 1835–1838, https://doi.org/10.1001/archopht.1982.01030040815023.
[12] J.C. Morrison, K.C. Swan, Descemet's membrane in penetrating keratoplasties of the human eye, Arch. Ophthalmol. 101 (1983) 1927–1929, https://doi.org/10.1001/archopht.1983.01040020929020.
[13] C. Boote, E.P. Dooley, S.J. Gardner, C.S. Kamma-Lorger, S. Hayes, K. Nielsen, J. Hjortdal, T. Sorensen, N.J. Terrill, K.M. Meek, Quantification of collagen ultrastructure after penetrating keratoplasty - implications for corneal biomechanics, PLoS One 8 (2013), https://doi.org/10.1371/journal.pone.0068166.
[14] J. Sugar, Experimental corneal wound strength, Arch. Ophthalmol. 92 (1974) 248, https://doi.org/10.1001/archopht.1974.01010010256018.
[15] B.E. McCarey, J.A. Napalkov, P.A. Pippen, J.M. Koester, T. Al Reaves, Corneal wound healing strength with topical antiinflammatory drugs, Cornea 14 (1995) 290–294, https://doi.org/10.1097/00003226-199505000-00010.
[16] P.I. Condon, D.W. Hill, The testing of experimental corneal wounds stitched with modern corneo scleral sutures: experimental corneal wound healing. I. Microsurgical and tensiometric techniques and results, Ophthalmic Res. 5 (1973) 137–150, https://doi.org/10.1159/000266033.
[17] A.R. Gasset, C.H. Dohlman, The tensile strength of corneal wounds, Arch. Ophthalmol. 79 (1968) 595–602, https://doi.org/10.1001/archopht.1968.03850040597020.
[18] A. Hjorth Simonsen, T.T. Andereassen, K. Bendix, The healing strength of corneal wounds in the human eye, Exp. Eye Res. 35 (1982) 287–292, https://doi.org/10.1016/S0014-4835(82)80053-5.
[19] F. Küng, D.W. Schubert, P. Stafiej, F.E. Kruse, T.A. Fuchsluger, A novel suture retention test for scaffold strength characterization in ophthalmology, Mater. Sci. Eng. C 69 (2016) 941–946, https://doi.org/10.1016/j.msec.2016.07.052.
[20] F. Küng, D.W. Schubert, P. Stafiej, F.E. Kruse, T.A. Fuchsluger, Influence of operating parameters on the suture retention test for scaffolds in ophthalmology, Mater. Sci. Eng. C 77 (2017) 212–218.
[21] ISO–71983, Cardiovascular implants and extracorporeal systems – Vascular prostheses – Tubular vascular grafts and vascular patches, Int. Organ. Stand. (2016), 2016.
[22] M. Pensalfini, S. Meneghello, V. Lintas, K. Bircher, A.E. Ehret, E. Mazza, The suture retention test, revisited and revised, J. Mech. Behav. Biomed. Mater. 77 (2018) 711–717.
[23] F. Küng, D.W. Schubert, P. Stafiej, F.E. Kruse, T.A. Fuchsluger, A novel suture retention test for scaffold strength characterization in ophthalmology, Mater. Sci. Eng. C 69 (2016) 941–946, https://doi.org/10.1016/j.msec.2016.07.052.
[24] H. Gururani, S.N.S.H. Chittajallu, M. Ramji, S. Basu, V. Chinthapenta, An in-vitro investigation on the birefringence of the human cornea using digital photoelasticity, Exp. Mech. (2022), https://doi.org/10.1007/s11340-022-00910-1.
[25] Standards of Eye Banking in India, 2020.
[26] A. Elsheikh, D. Wang, M. Brown, P. Rama, M. Campanelli, D. Pye, Assessment of corneal biomechanical properties and their variation with age, Curr. Eye Res. 32 (2007) 11–19, https://doi.org/10.1080/02713680601077145.
[27] A. Elsheikh, D. Alhasso, P. Rama, Biomechanical properties of human and porcine corneas, Exp. Eye Res. 86 (2008) 783–790, https://doi.org/10.1016/j.exer.2008.02.006.
[28] M. Ramji, K. Ramesh, Adaptive quality guided phase unwrapping algorithm for whole-field digital photoelastic parameter estimation of complex models, Strain 46 (2010) 184–194, https://doi.org/10.1111/j.1475-1305.2008.00431.x.
[29] H. Gururani, S.N.S.H. Chittajallu, R. Manoharan, S. Basu, V. Chinthapenta, Identification of subject-specific fibrillar disposition in healthy rabbit cornea through birefringence analysis, Opt Laser. Eng. 169 (2023) 107747, https://doi.org/10.1016/j.optlaseng.2023.107747.
[30] K. Tonsomboon, C.T. Koh, M.L. Oyen, Time-dependent fracture toughness of cornea, J. Mech. Behav. Biomed. Mater. 34 (2014) 116–123, https://doi.org/10.1016/j.jmbbm.2014.01.015.
[31] O.N. Serdarevic, K. Hanna, A.-C. Gribomont, M. Savoldelli, G. Renard, Y. Pouliquen, Excimer laser trephination in penetrating keratoplasty, Ophthalmology 95 (1988) 493–505, https://doi.org/10.1016/S0161-6420(88)33160-X.
[32] S.N.S.H. Chittajallu, H. Gururani, K.M. Tse, S.N. Rath, S. Basu, V. Chinthapenta, Investigation of microstructural failure in the human cornea through fracture tests, Sci. Rep. 13 (2023) 13876, https://doi.org/10.1038/s41598-023-40286-3.
[33] W. Yang, V.R. Sherman, B. Gludovatz, E. Schaible, P. Stewart, R.O. Ritchie, M.A. Meyers, On the tear resistance of skin, Nat. Commun. 6 (2015) 1–10, https://doi.org/10.1038/ncomms7649.
[34] A. Pissarenko, W. Yang, H. Quan, B. Poyer, A. Williams, K.A. Brown, M.A. Meyers, The toughness of porcine skin: quantitative measurements and microstructural characterization, J. Mech. Behav. Biomed. Mater. 109 (2020) 103848, https://doi.org/10.1016/j.jmbbm.2020.103848.
[35] C.T. Koh, M.L. Oyen, Branching toughens fibrous networks, J. Mech. Behav. Biomed. Mater. 12 (2012) 74–82, https://doi.org/10.1016/j.jmbbm.2012.03.011.
[36] D.J. Pettinelli, C. Starr E, W. Stark J., Late traumatic corneal wound dehiscence after penetrating keratoplasty, Arch. Ophthalmol. 123 (2005) 853, https://doi.org/10.1001/archopht.123.6.853.
[37] F. Beer, R.P. Patil, A. Sinha-Roy, B. Baumann, M. Pircher, C.K. Hitzenberger, Ultrahigh resolution polarization sensitive optical coherence tomography of the human cornea with conical scanning pattern and variable dispersion compensation, Appl. Sci. 9 (2019), https://doi.org/10.3390/app9204245.
[38] M.A. Kirby, G. Regnault, I. Pelivanov, M. O'Donnell, R. Wang, T.T. Shen, Non-contact acoustic micro-tapping optical coherence elastography for quantification of corneal anisotropic elasticity: in vivo rabbit study, ArXiv (2023).
[39] M.A. Kirby, I. Pelivanov, S. Song, Ł. Ambrozinski, S.J. Yoon, L. Gao, D. Li, T.T. Shen, R.K. Wang, M. O'Donnell, Optical coherence elastography in ophthalmology, J. Biomed. Opt. 22 (2017) 1, https://doi.org/10.1117/1.jbo.22.12.121720.
[40] Y. Wang, Y. Zhang, G. Shi, S. Ai, G. Liu, X. Han, X. He, Evaluation of Residual Corneal Stromal Bed Elasticity by Optical Coherence Elastography Based on Acoustic Radiation Force, Photonics 10 (2023) 266, https://doi.org/10.3390/photonics10030266.
[41] J.N. Webb, H. Zhang, A.S. Roy, J.B. Randleman, G. Scarcelli, Detecting mechanical anisotropy of the cornea using Brillouin microscopy, Transl. Vis. Sci. Technol. 9 (2020) 26, https://doi.org/10.1167/tvst.9.7.26.
[42] L. Asroui, H. Zhang, G. Scarcelli, J.B. Randleman, Comparison of Brillouin shifts between keratoconus, post-LASIK, and normal control corneas, Invest. Ophthalmol. Vis. Sci. (2022), 2398 – A0201-2398 – A0201.

[43] G. Scarcelli, R. Pineda, S.H. Yun, Brillouin optical microscopy for corneal biomechanics, Investig. Ophthalmol. Vis. Sci. 53 (2012) 185–190, https://doi.org/10.1167/iovs.11-8281.
[44] C. Cinton, L.C. Hassinger, C.L. Kublin, D.J. Cannon, Biochemical and ultrastructural changes in collagen during corneal wound healing, J. Ultrasructure Res. 65 (1978) 13–22, https://doi.org/10.1016/S0022-5320(78)90017-5.
[45] D.M. Maurice, F. Monroe, Cohesive strength of corneal lamellae, Exp. Eye Res. 50 (1990) 59–63, https://doi.org/10.1016/0014-4835(90)90011-I.
[46] J.C. Larson, M.L. Raven, H.D. Potter, Traumatic loss of a healed corneal button, Ophthalmology 123 (2016) 753, https://doi.org/10.1016/j.ophtha.2016.01.040.